

# Two-dimensional Synchrotron Beam Characterisation from a Single Interferogram

Bojan Nikolic\*

*Cavendish Laboratory, University of Cambridge, Cambridge CB3 0HE, UK*

Christopher L. Carilli

*National Radio Astronomy Observatory, P. O. Box 0, Socorro, NM 87801, US*

Nithyanandan Thyagarajan

*Commonwealth Scientific and Industrial Research Organisation (CSIRO),  
Space & Astronomy, P. O. Box 1130, Bentley, WA 6102, Australia*

Laura Torino<sup>†</sup> and Ubaldo Iriso

*ALBA - CELLS Synchrotron Radiation Facility*

*Carrer de la Llum 2-26,*

*08290 Cerdanyola del Vallès (Barcelona), Spain*

(Dated: 17 May 2024)

Double-aperture Young interferometry is widely used in accelerators to provide a one-dimensional beam measurement. We improve this technique by combining and further developing techniques of non-redundant, two-dimensional, aperture masking and self-calibration from astronomy. Using visible synchrotron radiation, tests at the ALBA synchrotron show that this method provides an accurate two-dimensional beam transverse characterisation, even from a single 1 ms interferogram. The non-redundancy of the aperture mask in the technique enables it to be resistant to spatial phase fluctuations that might be introduced by vibration of optical components, or in the laboratory atmosphere.

## I. INTRODUCTION

Two-dimensional (2D) beam size measurements in the transverse plane are of fundamental importance to quantify the performance of accelerators. They allow for the characterization of the emittance of the particle beam, a key parameter defining an accelerator. The transverse distribution of particles is well characterized by a 2D Gaussian [1] and parameterised by major axis, minor axis, and the tilt angle.

In synchrotron light sources, noninvasive beam size measurements exploiting the Synchrotron Radiation (SR) emitted by the electron beam are mainly performed via direct imaging or interferometry techniques [2]. Among the direct imaging techniques, the X-ray pinhole [3] is widely used in synchrotron light sources as it directly provides a 2D image of the source. A recent design study for X-ray pinhole cameras can be found in [4].

At longer wavelengths the direct imaging is limited by diffraction and interferometric techniques are preferred. Among them, the two-aperture interferometer [5] is widely used in accelerators, but it only provides a one dimensional measurement in the direction of the orientation of the apertures. Full 2D beam reconstruction can be obtained by a series of measurements, rotating the aperture mask between measurements [6], but at least

four orientations are needed. A four-aperture square interferometric mask layout [7] has been used to obtain a 2D source size from a single interferometric measurement, but such a mask layout suffers from decoherence due to redundant sampling in Fourier space [8]. Moreover, the non-uniformity of aperture illumination across the mask due to the intrinsic distribution of the synchrotron radiation can irrecoverably corrupt the results [9]. Redundant two-dimensional mask interferometry at X-ray wavelengths has also been proposed [10] but similarly it will not be able to recover the relative phases and illuminations of the individual apertures.

In the last years several techniques are arising to guarantee high resolution and fast measurement needed from the upcoming 4th generation of synchrotron light sources [11, 13, 14].

In this paper we propose the combination of Non Redundant Aperture (NRA) mask interferometry in combination to gain fitting [15, 16], two technique broadly used in astronomy separately and united here for the first time. This combination provides a full transverse characterization of the electron beam in a single acquisition, using the visible part of the synchrotron radiation. The main components of the optical setup are out of vacuum and data is acquired using a standard CCD. The analysis can be performed online and results can be used in a feedback loop to guarantee a stable emittance in both planes

In this paper, we present the technique in detail and use it to characterize the ALBA electron beam.

One alternative method of two-dimensional constraint on the synchrotron beam size at X-ray wavelengths is by

---

\* E-mail:bn204@cam.ac.uk

† E-mail: ltorino@cells.es

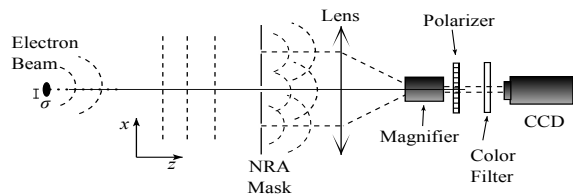


FIG. 1. Schematic diagram of the experimental setup.

measuring the power spectrum of speckle formed by a random scattering medium [11], an approach also used in astronomy [12]. Like our approach, speckle also depends on the interference of the synchrotron radiation but unlike the present method, speckle power spectrum only contains information about the amplitude of the coherence function and requires operation with X-rays in a vacuum for sufficient resolution.

While angular resolution of direct imaging at visible wavelengths is limited, it is possible to improve the achieved transverse resolution by placing a high-accuracy lens physically close to the radiation source [13]. This approach, however, needs to deal with the intense X-ray flux, be implemented largely in vacuum, and is difficult in the next-generation synchrotrons which have narrow radiation extraction angles due to space constraints.

Finally, in some cases it is possible to use detailed measurement of the angular distribution of the spectrum of the emitted synchrotron radiation to infer the dimensions of the particle beam [14].

## II. EXPERIMENTAL SETUP

The experiments were carried out at the ALBA synchrotron facility. The laboratory optical bench setup and the imaging camera were similar to the two-aperture interferometry described by [6], except that we use new multi-aperture masks and different integration times.

The visible part of the synchrotron radiation, emitted from a bending magnet, is extracted by an in-vacuum mirror positioned at a distance of 8.64 m. The mirror captures only the upper lobe of the radiation, cutting the wavefront 10 mm above the orbit plane. The light then passes through a vacuum window and is transported to the beamline optical table via 7 additional mirrors, covering a total optical path from the source of approximately 15 m [17]. After diffraction by the NRA mask and focusing with a 0.5 m focal length lens, the image is magnified, filtered using a  $538 \pm 10$  nm color filter, polarized to select  $\sigma$  polarization, and finally captured by a CCD camera. A sketch of the experiment is illustrated in Fig. 1.

We present source size measurements made using a

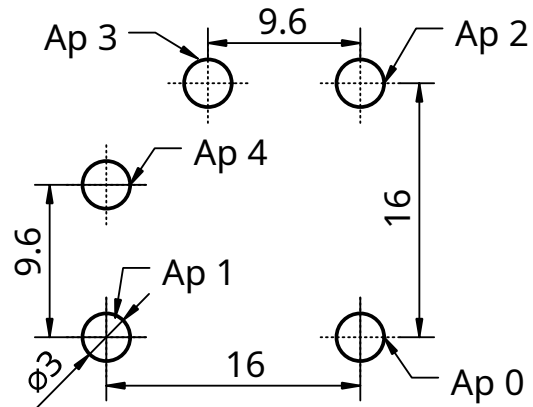


FIG. 2. Drawing of the non-redundant mask with aperture labels as used for labelling baselines. (All dimensions in millimetres).

five-aperture mask designed such that the vector (‘baseline’) between every pair of apertures is unique (a ‘non-redundant’ mask). This means that each spatial frequency in the Fourier domain is measured by only a single pair of apertures in the plane of the mask, thereby avoiding decoherence that would occur for redundant aperture measurements in the presence of phase errors. This mask was an adaptation of the non-redundant array in [18], with the five apertures selected to maximize the longer baselines (given the source is only marginally resolved) while fitting within the illuminated area.

The geometry of the mask is shown in Fig. 2. The hole sizes were 3 mm in diameter and the mask was machined out of aluminium to high accuracy in the ALBA mechanical workshop (better than 0.1 mm).

## III. MEASURING VISIBILITIES

Data are acquired as CCD two-dimensional arrays of size  $1296 \times 966$ . We first remove the constant offset which is due to a combination of the bias and the dark current. We use a fixed estimate of this offset obtained by examination of the darkest areas of the CCD, as well as from the FFT of the image. Errors in this procedure accumulate in the central part of the FFT and contribute to the overall uncertainty of the beam reconstruction.

Next we pad and center the data so that the centre of the Airy disk-like envelope of the fringes set by the hole diameter is in the centre of a larger two-dimensional array of size  $2048 \times 2048$ . To find the correct pixel to center to, we first filter the acquired image with a wide (50 pixel) Gaussian kernel, then select the pixel with highest signal value. The Gaussian filtering removes the fringes leaving the remaining signal approximately corresponding to

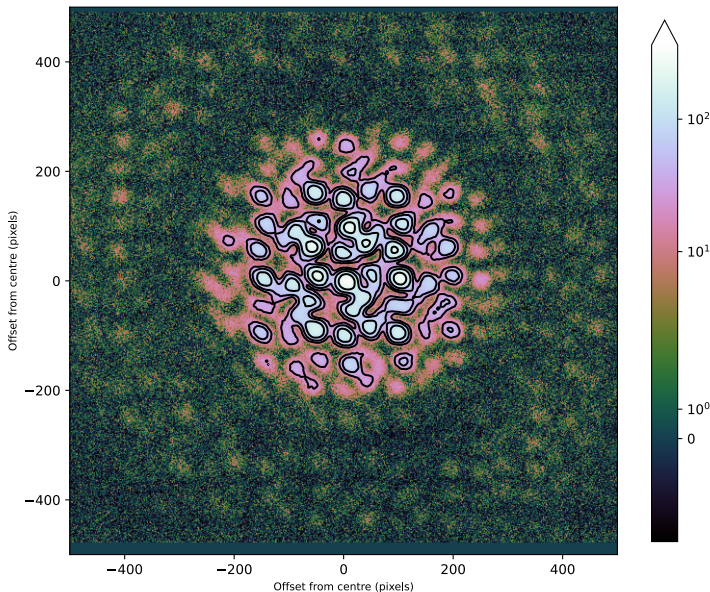


FIG. 3. Interferogram with five 3 mm-diameter holes and 1 ms integration time. The CCD image is bias-subtracted and centered. Contours are power-law in  $2^{-n}$ .

the fringe envelope. Without the filtering, the particular central pixel selected would be affected by the fringe position and the photon noise, rather than the envelope.

An example CCD frame processed in this way is shown in Fig. 3. The primary and first side lobe of the Airy disk envelope of the fringes can be seen. The measurement has high signal-to-noise with the fringes even in the first side-lobe clearly discernible above the noise.

To calculate the visibilities, we use the Fraunhofer diffraction integral, and the result that the Fourier transform of an intensity image is the auto-correlation of the field in the aperture plane. We therefore compute the two-dimensional Fourier transform of the padded CCD frame using the FFT algorithm. Amplitude of an example Fourier transform of an ALBA image is shown in Figure 4. Distinct peaks can be seen in the FFT amplitude corresponding to each baseline (i.e., vector) between the apertures in the mask.

We extract the visibilities on each of the baselines by calculating the complex sum of pixels within a circular aperture of radius 7 pixels, centered at the calculated position of the baseline. With the array padding used here, 1 mm on the mask corresponds to 2.54 pixels in the Fourier transformed interferogram and the correlated signal is expected up to twice the hole radius so the 7 pixel aperture captures almost all of the signal while minimizing noise and systematics. The resulting complex sum

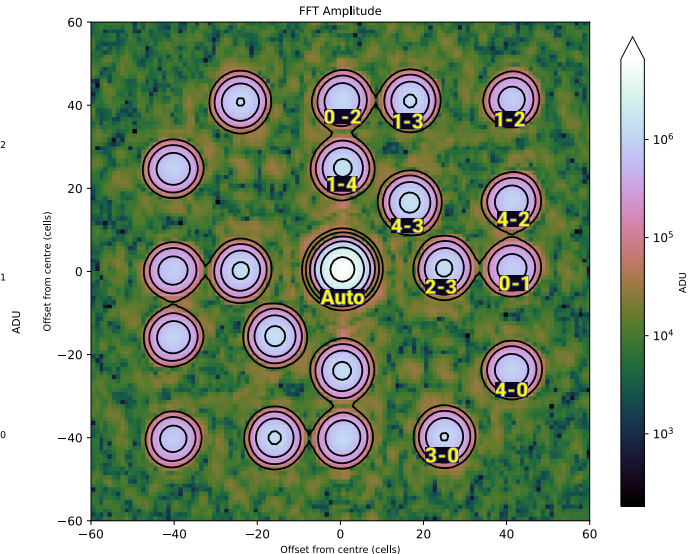


FIG. 4. Amplitude of the FFT of the sample interferogram in Figure 3, contours drawn at  $2^{-n}$  intervals relative to image maximum. Labels identify peaks of amplitude with the pair of apertures forming the baseline of visibility that the peak represents.

value contains both the amplitude and phase of the visibility.

#### IV. FITTING THE COHERENCES

The measured visibilities  $\|V_{ij}\|$  are a function of both the degree of coherence  $\gamma(u_{ij}, v_{ij})$  and the amplitudes of the electromagnetic radiation passing through each of the apertures  $\|G_i\|$ ,  $\|G_j\|$ , where  $i$  and  $j$  are indices of the apertures:

$$\|V_{ij}\| = \gamma(u_{ij}, v_{ij})\|G_i\|\|G_j\|. \quad (1)$$

Since it is not possible to ensure the intensity of radiation through the apertures are all the same, our strategy is to simultaneously fit for both the coherences as well as the 'gains' that correspond to the square root of intensity of the incident radiation at each of the apertures. If this fitting is not performed, errors introduced by non-uniform illumination are greater in the multi-aperture interferometry than in the two-aperture case because we only have a constraint on the total power of the radiation through all the apertures, not on the particular two apertures forming each visibility. This means that without fitting, a fractional difference in illumination of  $\epsilon$  leads to an error in coherence of order  $\epsilon^2$  in the two-aperture case but order  $\epsilon$  in the multi-aperture case. Furthermore, while with two holes it possible to position them so that

difference in illumination is minimised, this is impractical with five holes.

The central peak of the Fourier transform brings information on the auto-correlation and adds another constrain to the fit being the total signal being the sum of all the gains:

$$\|V_{\text{auto}}\| = \sum_i \|G_i\|^2. \quad (2)$$

### A. Parametrisation of the model for the coherence

By suitable approximations of the van Cittert–Zernike theorem (cite TMS 2017), the coherence can be very well represented by the Fourier transform of the source intensity distribution. Working on the assumption that the source is a multi-variate Gaussian [1], then the coherence is also a multi-variate Gaussian, which is what we use as the model. We fit a parametrisation in terms of the overall width ( $\sigma$ ) and the distortion in the vertical-horizontal directions ( $\eta$ ) and diagonal ( $\rho$ ) directions:

$$\gamma(u, v) = \exp\left[-\frac{(u^2 + v^2) + 2\rho(uv) + \eta(u^2 - v^2)}{2\sigma^2}\right] \quad (3)$$

and the independent variables  $u$  and  $v$  are coordinates of a displacement in the plane of the aperture mask. In this parametrisation in the plane of the aperture mask the major axis  $\sigma_u^0$ , minor axis  $\sigma_v^0$ , and the tilt angle  $\phi$  of the major axis  $\phi$  as measured from  $u$  direction are:

$$\sigma_u^0 = \sigma \left(1 - \sqrt{\eta^2 + \rho^2}\right)^{-\frac{1}{2}} \quad (4)$$

$$\sigma_v^0 = \sigma \left(1 + \sqrt{\eta^2 + \rho^2}\right)^{-\frac{1}{2}} \quad (5)$$

$$\phi = \tan^{-1} \left( \frac{\rho}{\eta - \sqrt{\eta^2 + \rho^2}} \right). \quad (6)$$

This is a convenient parametrisation for fitting as it avoids trigonometric functions and has low covariance of parameters in typical situations.

### B. Likelihood function

Under the assumption of normally distributed uncorrelated errors in the visibility measurements the likelihood is:

$$-\log(L) = \frac{\|V_{\text{auto}}^{\text{obs}} - V_{\text{auto}}^{\text{mod}}\|^2}{\xi_{\text{auto}}^2} + \sum_{i=0}^{N-2} \sum_{j=i+1}^{N-1} \frac{\|V_{ij}^{\text{obs}} - V_{ij}^{\text{mod}}\|^2}{\xi_{\text{vis}}^2} \quad (7)$$

where,  $N$  is the number of apertures in the mask (5 in this case),  $\|V_{ij}\|$  are the visibilities (Eq 1),  $\|V_{\text{auto}}\|$  is the total power (Eq (2)), and  $\xi_{\text{auto}}$  and  $\xi_{\text{vis}}$  are the estimates of uncertainty for the total power (or autocorrelation)

and visibility measurements, respectively. We estimated the uncertainty,  $\xi_{\text{vis}}$ , by making multiple samples in the Fourier transformed plane (i.e., the data shown in Figure 4) at positions which were not close to the visibility peaks. These parts of the visibility plane for which the input light is blocked by the optical system (the objective or the aperture mask) and hence contain only the random uncorrelated noise produced within the CCD. Variance between these samples is a good estimate of the random uncertainty on the visibility measurement. For  $\xi_{\text{auto}}$ , we add an additional 1% relative uncertainty due to systematic effects such as the bias subtraction that tend to accumulate in the total power measurement.

### C. Minimisation procedure

The best-fitting model was found by maximising the likelihood using the Levenberg–Marquardt algorithm with a numerically evaluated Jacobian. The fitting processing time is dominated by the Fourier transform computations and can be completed in around 25ms on a server-class CPU (dual Intel Xeon 8276), faster than the typical CCD read-out time. This means that, although in present experiments we analysed the data offline, the technique could be used for a system implemented for beam characterisation with low and predictable latencies typically dominated by the fixed latency of the CCD readout, i.e., near real-time measurement.

## V. RESULTS

We obtained a number of measurement runs on 2023-06-14 with 3 mm and 5 mm apertures, and with 1 ms and 3 ms integration times. Each run consisted of 30 CCD frames separated by one second. Data with 3 mm apertures and 1 ms integration time have the least time variation and highest apparent coherences indicating that it is of best quality [8].

### A. Beam size measurement

Using the 1 ms integration time data, we analysed each frame to derive both the illumination through each mask hole and the best fitting values for the coherences. The coherences are then used to calculate the size of the major axis of the electron beam using:

$$\sigma_{\text{major}} = \frac{\lambda L}{2\pi\sigma_v^0}, \quad (8)$$

where  $\lambda = 538$  nm and  $L = 15$  m as described in Section II. An analogous equation holds for the minor axis. The angle of the major axis of the beam is rotated by 90 degrees compared to the angle of the major axis of the coherence function given in Eq (4).

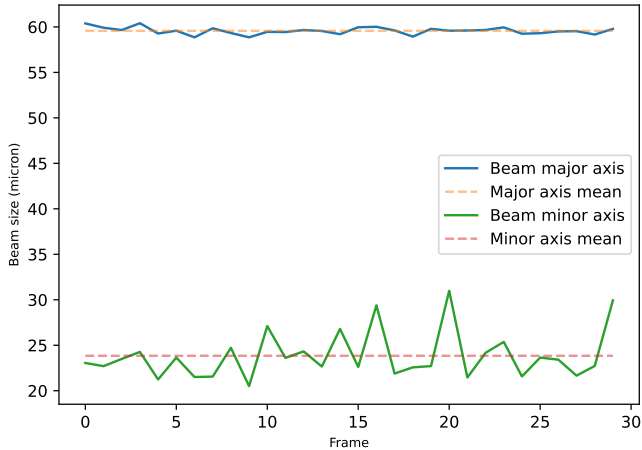


FIG. 5. Time series of measured beam major and minor axes,  $\sigma$ , from 30 interferogram frames each separated by one second. Dash lines are mean values.

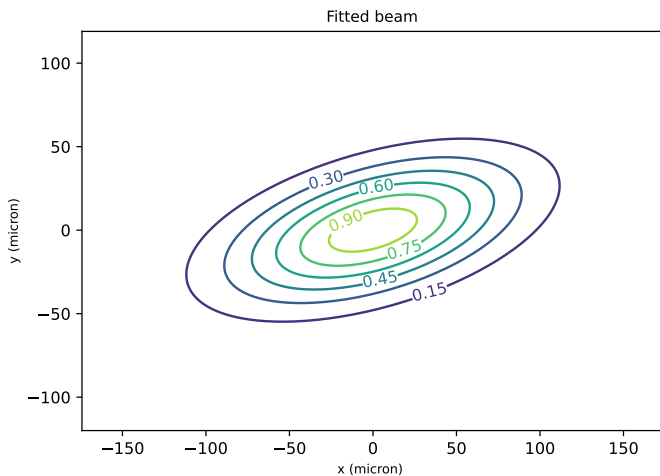


FIG. 6. Full 2D beam reconstruction from the average of 30 frames each 1 ms integration time.

The time series of these measurements, shown in Fig. 5, show high stability and repeatability, with an rms scatter of  $0.4 \mu\text{m}$  and  $2.6 \mu\text{m}$  in beam major and minor axes, respectively, and  $0.9^\circ$  in the angle. The final beam derived is the average of the time series, which is shown in Fig. 6. The mean estimate of the axes sizes is  $\sigma_{\text{major}} = 59.6 \mu\text{m} \pm 0.1 \mu\text{m}$  and  $\sigma_{\text{minor}} = 23.8 \mu\text{m} \pm 0.5 \mu\text{m}$ . The error on the minor axis is larger because of its significantly smaller size, and also because the available baselines are shorter, being limited by the size of the illuminated region. The angle the major axis makes with the horizontal is  $15.9^\circ \pm 0.2^\circ$ .

Method	Major ( $\mu\text{m}$ )	Minor ( $\mu\text{m}$ )	Tilt Angle
2ap (3 ms)	$61.7 \pm 1.5$	$25.5 \pm 1.5$	$16.6^\circ$
5ap (1 ms)	$59.6 \pm 0.1$	$23.8 \pm 0.5$	$15.9^\circ \pm 0.2^\circ$
LOCO	57.5	20.6	$14.9^\circ$
Pinhole	58.5	24.6	$14.9^\circ$

TABLE I. Comparison of beam size measurements by various methods. 2ap: two-aperture rotated mask. 5ap: the present five-aperture method. LOCO: ideal value based on the analysis of the magnet lattice of ALBA [19]. Pinhole: beam size inferred from the emittance calculation at the ALBA x-ray pinholes, although at a different location in the ring [20].

## B. Comparison with other methods

On the same day we also obtained measurements using rotated two-aperture SRI as described by [6]. This method has previously been shown to be reliable and uses a different fitting procedure to obtain the beam sizes. Those measurements were obtained with 3 ms integration time (in order to achieve similar SNR with less overall light throughput), and so we compare them against the analysis of the five-aperture interferometry in Table I. As for the 5 apertures, the two-aperture SRI measurements employed 30 consecutive frames in each of four rotated positions of the mask. These rotated positions are required to perform the full 2D characterization in this method.

Table I also shows the expected results for horizontal and vertical beam size and the tilt angle at the synchrotron radiation extraction point obtained using Linear Optics from Closed Orbits (LOCO, [19]). LOCO is a tool to measure and correct the orbit of a circular accelerator. It takes into account several measurements of the machine, such as current in magnets and BPM readings, and models them to estimate the expected beam behavior. The obtained result is not necessarily exact but indicative. We also list the beam size inferred from the emittance values measured by the two X-ray pinholes at ALBA [20], and the expected Twiss parameters at the source size of the NRA experiment.

Table I shows consistency within the errors between the 5-hole, 2-hole and pinhole beam size measurements. The SRI measurements are also within 4% to 20% of the LOCO modeling, depending on parameter.

## VI. RANDOM AND SYSTEMATIC ERRORS

Our error estimates on measured quantities in Table I are empirical, based on the variance in a sequence of 30 measurements. In this section we look further at random and potential systematic errors in our technique.

The fundamental limit to accuracy comes from the photon counting statistics. These follow the Poisson distribution where the standard error for large count rates is the square root of the number of photons. Based on the

measured counts in the visibilities, we estimate this error to be small, a relative error of  $\leq 0.2\%$ . For reference, we have performed an analysis of the fitting process and find that a relative random error of  $\sim 1\%$  in the coherences per frame would lead to the empirically measured scatter of the fitted beam quantities from the time series.

There are also a number of potential systematic errors which we estimate here together with our correction and mitigation strategy.

First, we demonstrate the importance of gain self-calibration to correct for the non-uniform illumination across the mask, as defined in Equation 5. The gains,  $\|G_i\|$ , derived for the 5 holes over the 30 time records are shown in Figure 7. The gains are stable to  $\leq 1\%$  over the 30 records, but the values vary from hole to hole by up to 25% (which implies a  $\sim 50\%$  change in power of the illumination across the mask). This is due to unavoidable differences in the illumination from the beam across the mask, in part due to the inherent vertical intensity distribution of the synchrotron light and in part due to Fraunhofer diffraction produced by various mirror edges.

We quantify the impact of this gain variation by an alternate fit for the source size without correcting the visibility amplitudes by the gains. In this analysis the derived source major axis is too large by typically 15%, and the position angle and minor axis sizes are wrong by a factor 2 or more. The sensitivity of the minor axis to the gain corrections reflects the fact that this axis is only marginally resolved by our longest baseline, and hence true coherences are high, 90% or more, such that even small corrections to the measured visibilities lead to substantial changes in fitted beam minor axis. Further, the agreement between the gain-corrected beam size and the expected beam size from other methods lends confidence that the gain correction process is valid.

The gains can alternatively be determined by closing in turn all but one of the holes on the mask and measuring the flux received at the CCD. Such a sequential measurement of total power received is sensitive to effects such as variation in the read noise of the CCD and the intensity of the synchrotron radiation. Furthermore the measurement would not be accurate after any appreciable change in the position or orientation of the mask since the illumination pattern on the mask has diffraction features on scales comparable to the hole sizes. This approach is hence less convenient for routine use but is a good way to check the approach in which the gains are fitted directly with the source and we are in the process of performing these tests at ALBA.

We also investigated how specific parameter choices in our approach affect the measured visibilities, which gives an illustration of the residual systematic error may be. The following were investigated:

- Not centering the image on the Airy disk before Fourier transforming to the  $uv$  plane leads to changes in visibilities in range  $\sim 1\%$ – $4\%$ , due to a phase ramp across the region of  $uv$  plane over which the visibilities are measured.

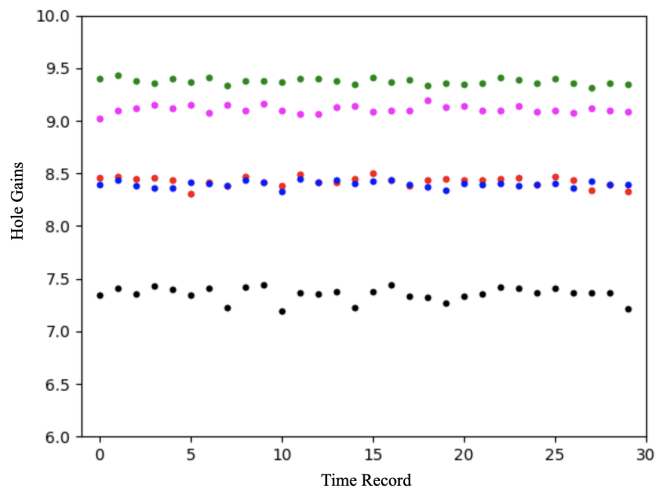


FIG. 7. Solutions for the hole gain amplitudes for each hole for the 30 frames, as defined in equation 5. The units of the gains are in  $\text{root}(\text{counts})/10^3$ , and derived such that the resulting coherences are normalized to unit peak. black = Ap0; red = Ap1; blue = Ap2; green = Ap3; Purple = Ap4.

- Changing the radius for summing the complex visibilities in the  $uv$  plane from 3 to 9 pixels changes the coherences by  $\leq 2\%$ .
- Changing the hole size from 5 mm to 3 mm raises the coherences in range  $\sim 5\%$ – $10\%$
- Changing the frame time from 3ms to 1ms raises the coherences by  $\sim 1\%$ – $8\%$ .
- Not removing a mean frame bias lowers coherences  $\sim 2\%$ .

The large impact of the hole size and integration time suggests de-correlation on longer length and time scales, which could be due to air turbulence in the lab or vibration of some parts of the instrument or optical chain. The impact of other parameters show that a careful analysis and calibration is needed if the theoretical noise limit is to be achieved.

Finally, we demonstrate the importance of using a non-redundant mask by repeating the experiment with redundant mask and comparing the results. For this test, a six hole mask was employed, identical to the current 5 hole mask, but including the fourth corner hole, such that we now have two redundant baselines: the two 16mm horizontal baselines and two 16mm vertical baselines. Figure 8 shows the results for six of the baselines, including the two redundant baselines. We find the RMS scatter on the redundant baselines is much higher, by a factor 3 to 5, likely arising from time varying decoherence due to phase fluctuations, and that the mean amplitude is lower by about 5% than expected using the non-redundant 5 hole mask.

The current experiment is simply a demonstration of the technique, which is apparently verified by the good



## VII. CONCLUSIONS

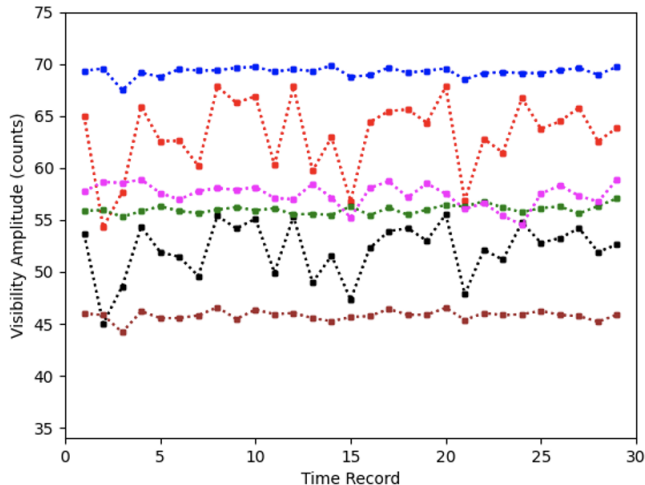


FIG. 8. Time series of some of the visibility amplitudes for a 6 hole mask in which two of the visibilities (horizontal 16mm and vertical 16mm), are measured with redundant baselines (red and black curves), while the rest are for non-redundant baselines. The visibility amplitude axis is in units of  $10^6$  counts.

agreement between the results from this technique with three other independent techniques for beam size measurements. We are continuing these investigations in order to improve the performance. For next-generation instruments, the ultimate resolution limit,  $\delta\theta$ , is set by the signal-to-noise ratio and the interferometric fringe spacing of the maximum baseline,  $B_{\max}$ , of the mask:  $\delta\theta \sim \theta_{B_{\max}}/(S/N)$ , where  $\theta_{B_{\max}} \sim \lambda/B_{\max}$  (see Fomont in [21] equ 14-5). In our practical case at ALBA, for a typical  $B_{\max}=20$  mm,  $S/N=0.2\%$  and averaging 30 frames, the ultimate resolution becomes  $\delta_X \sim 0.1 \mu\text{m}$ , consistent with best error estimate from variance between frames shown in Table I.

We are in the process of improving our SRI technique through masks with more apertures over a larger area of the beam footprint on the mask, shorter integration times and hole size, and decreasing the measurement wavelength. Based on the various errors and uncertainties discussed above, we feel coherence measurement below 1% of the true values are plausible. In general, future SRI optical systems would benefit from allowing for longer baselines (larger photon beam footprints on the mask), and shorter wavelengths, implying higher resolution. Extension of the technique to much shorter wavelengths, even to the EUV, is feasible, although focusing optics become more of a challenge, as does mask production.

The particle beam can be well characterised using a single interferogram using the emitted synchrotron radiation and a simple apparatus with no moving parts. The relatively large CCD image data set can be processed without iterative model-fitting to derive a much smaller data set of visibilities (in our case 10), which are then input into a fitting procedure. Importantly, this model fitting needs to fit for both the differential illumination of the apertures as well as for the coherences. The overall processing complexity is low and suitable for near-real time applications. The beam parameters and uncertainty in a single acquisition with a 5-hole non-redundant mask are comparable to those obtained with the two-aperture method employing multiple acquisitions with rotation of the aperture. The larger amount of light let through by the five apertures contributes to the efficiency of the technique.

A key aspect of the technique is the use of non-redundant aperture mask which means that the visibility between each pair of apertures is measured separately. This means that distortions in the incoming wavefront at the aperture plane can be measured as function of position in the plane as well as a function of time (the latter by taking frames with short enough integration time). The spatial fluctuation of the incoming wavefront can be both in amplitude (which is the seen as the uneven illumination pattern on the mask) or in phase (e.g., due to atmospheric turbulence or optics vibrations). As discussed in Section VI, both of these errors are significant. Although characterising a Gaussian function does not make use of the measured phases, it is still susceptible to phase errors across the aperture mask if visibilities with different phase errors are combined as they are in a redundant mask or filled aperture system.

Therefore by use of a non-redundant mask, and by making the individual apertures small enough and the integration times short enough, it is possible to at least reduce the effects of both amplitude and phase errors which vary in position, time or a combination of both. In order for the model and the  $\|G_i\|$  values to be well constrained, there must be more measured visibilities than the sum of the number of apertures and the number of model free parameters [16]. This is satisfied with 5 apertures for the Gaussian model of the synchrotron beam. More complex models are possible, e.g., in astronomical applications it is also routine to iteratively build up a model when there is a significant number of measurements and the source plane can be assumed to sparse [16]. In these cases, a larger number of apertures would be needed.

The technique presented can likewise be used for efficient and rapid characterisation of other high-intensity light sources even after propagation through a medium inducing phase and amplitude fluctuations. Moreover, the complex visibilities and  $G_i$  values encode precise information on the optical performance of the system. For example, the static phases of  $G_i$  are a direct measure of

wavefront phase error accumulated in the optical system up to the aperture mask and hence can be used to infer the error in larger optical components. Slowly varying phases of  $G_i$  after a change in experimental condition can be used to, for example, measure the deformation of the optical system due to thermal expansion/contraction.

The technique presented here is a good demonstration of interdisciplinary science, applying astronomical interferometric techniques to accelerator physics.

**Acknowledgments.** The National Radio Astronomy Observatory is a facility of the National Science Foundation operated under cooperative agreement by Associated Universities, Inc. Patent applied for: UK Patent Application Number 2406928.8, USA Applications No. 63/648,303 (RL 8127.306.USPR) and No. 63/648,284 (RL 8127.035.GBPR). We thank two anonymous referees for their comments which have improved the paper presentation.

- 
- [1] M. Sands, The Physics of Electron Storage Rings: An Introduction, Conf. Proc. C **6906161**, 257 (1969).
- [2] G. Kube, Review of Synchrotron Radiation Based Diagnostics for Transverse Profile Measurements, in *Proceedings of DIPAC07, Venice (Italy)* (2007).
- [3] P. Elleaume, C. Fortgang, C. Penel, and E. Tarazona, Measuring Beam Sizes and Ultra-Small Electron Emittances Using an X-ray Pinhole Camera, *Journal of Synchrotron Radiation* **2**, 209 (1995).
- [4] A. Trebushinin, G. Geloni, S. Serkez, R. Khubbutdinov, and E. Saldin, Pinhole camera for electron beam size diagnostic at storage ring with an ultralow emittance, *Phys. Rev. Accel. Beams* **27**, 032802 (2024).
- [5] T. Mitsuhashi, Beam profile and size measurement by SR interferometers, in *Joint US-CERN-Japan-Russia School on Particle Accelerators: Beam Measurement* (1998) pp. 399–427.
- [6] L. Torino and U. Iriso, Transverse beam profile reconstruction using synchrotron radiation interferometry, *Phys. Rev. Accel. Beams* **19**, 122801 (2016).
- [7] M. Masaki and S. Takano, Two-dimensional visible synchrotron light interferometry for transverse beam-profile measurement at the SPring-8 storage ring, *Journal of Synchrotron Radiation* **10**, 295 (2003).
- [8] C. Carilli, B. Nikolic, L. Torino, U. Iriso, and N. Thyagarajan, *Deriving the size and shape of the ALBA synchrotron light source with optical aperture masking: technical choices*, Tech. Rep. (ALBA, 2024).
- [9] A. Novokshonov, G. Kube, and A. Potylitsyn, Two-Dimensional Synchrotron Radiation Interferometry at PETRA III, in *8th International Particle Accelerator Conference* (2017).
- [10] Q. Li, Y. Lu, Y. Lu, and P. Wang, Two-dimensional spatial coherence measurement of x-ray sources using aperture array mask, *Opt. Express* **31**, 36304 (2023).
- [11] M. Siano, B. Paroli, M. A. C. Potenza, L. Teruzzi, U. Iriso, A. A. Nosych, E. Solano, L. Torino, D. Butti, A. Goetz, T. Lefevre, S. Mazzoni, and G. Trad, Two-dimensional electron beam size measurements with x-ray heterodyne near field speckles, *Phys. Rev. Accel. Beams* **25**, 052801 (2022).
- [12] A. Labeyrie, Attainment of Diffraction Limited Resolution in Large Telescopes by Fourier Analysing Speckle Patterns in Star Images, *A&A* **6**, 85 (1970).
- [13] M. Labat, O. Chubar, J. Breunlin, N. Hubert, and A. Andersson, Bending magnet synchrotron radiation imaging with large orbital collection angles, *Phys. Rev. Lett.* **131**, 185001 (2023).
- [14] Curcio *et al.*, Reconstruction of lateral coherence and 2d emittance in plasma betatron x-ray sources, *Scientific Reports* **14** (2024).
- [15] C. A. Haniff, C. D. Mackay, D. J. Titterton, D. Sivia, and J. E. Baldwin, The first images from optical aperture synthesis, *Nature* **328**, 694 (1987).
- [16] F. R. Schwab, Processing of three-dimensional data, in *1980 International Optical Computing Conference I*, Society of Photo-Optical Instrumentation Engineers (SPIE) Conference Series, Vol. 231, edited by W. T. Rhodes (1980) p. 18.
- [17] U. Iriso and F. Fernandez, in *ALBA Project Document Report No. AAD-FE-DI-VMIR-01* (2011).
- [18] A. I. González and Y. Mejía, Nonredundant array of apertures to measure the spatial coherence in two dimensions with only one interferogram, *J. Opt. Soc. Am. A* **28**, 1107 (2011).
- [19] J. Safranek, Experimental determination of storage ring optics using orbit response measurements, *Nuclear Instruments and Methods in Physics Research Section A: Accelerators, Spectrometers, Detectors and Associated Equipment* **388**, 27 (1997).
- [20] U. Iriso, Z. Marti, A. Nosych, A. Cazorla, and I. Mases, PSF Characterization of the ALBA X-Ray Pinholes, in *Proceeding of IBIC2022* (2022).
- [21] C. L. Taylor, G. B. and Carilli and R. A. Perley, eds., *Synthesis Imaging in Radio Astronomy II*, Vol. 180 (ASP Conference Series, 1999).